Correspondence

Order Selection Criteria for Detecting Mean Scatterer Spacings with the AR Model

Tomy Varghese, Kevin D. Donohue,
Vlad I. Genis, and Ethan J. Halpern

Abstract— **This paper examines the detection of regular scatterer spacings from backscattered ultrasound using the autoregressive (AR) cepstrum. Monte Carlo simulations present a relationship between the probability of detection and the AR model order. An example using liver tissue data supports the observations made in the simulation.**

I. Introduction

Since ultrasound waves interact closely with tissue structures, information in the backscattered signal can potentially be used to identify and monitor diseases that change such structures. This paper examines the performance of the autoregressive (AR) model cepstrum in detecting mean scatterer spacings from tissue where two types of scattering structures exist, regular and diffuse (speckle scatterers). Scattering of this nature is observed in liver tissue, where the portal triads contribute to the regular (quasi-periodic) scattering with a spacing near 1 mm, while speckle or diffuse scattering is generated from the many small scatterers randomly distributed throughout the tissue [1].

The mean scatterer spacing parameter has been used by various investigators to characterize tissue with regular structures [2]–[11]. Fellingham and Sommer measured the mean scatterer spacing in normal and diseased liver and spleen tissue. They demonstrated a measurable change in the mean scatterer spacing for tissues with different pathology [2]. Mean scatterer spacing has also been used by Garra *et al.* in their multifeature classification of diffuse liver disease [3]. Landini and Verrazzani classified normal and diseased tissue based on the regularity in the scatterer distribution. The mean scatterer spacing and its variance was used to classify tissue architecture [4]. Landini and Verrazzani report standard deviations for regular scatterer distributions in biological tissue range from 10.5%, for normal uterus tissue, to 15.8%, for tissue with an intermediate structure (sclerosing adenosis in breast tissue) [4].

Mean scatterer spacing has been estimated from intensity scans using the autocorrelation function [7], [8], and from RF scans using cepstral [4]–[6] and spectral correlation [9]–[11] techniques. Cepstral methods use the inverse Fourier transform of the logarithm of the power spectrum to separate the slow variations in the magnitude spectrum due to the system response from the rapid variation due to the periodicities of the scatterer spacings. After windowing out from the cepstrum the system effects that occur within the resolution limit of the system, the location of the largest peak corresponds to the mean scatterer spacing. Wear *et al.* [6] proposed using an AR cepstral technique (based on the Burg's algorithm for AR parameter estimation), and demonstrated a superior performance over cepstral methods using the periodogram, especially when smaller gate lengths were used. While it has been shown that spectral correlation methods are more robust than the AR cepstrum when detecting a broad range of scatterer spacings [11], the AR cepstrum has the advantage of higher resolution estimates (independent of the sampling grid). In addition, the performance of the AR cepstrum is reasonably reliable in cases where the range of scatterer spacings is limited and the order of the AR model is chosen to span a distance slightly larger than the largest spacing in that range. Thus, this approach can be particularly useful for detecting small changes in scatterer spacings, such as those due to tissue swelling or temperature changes. It can also be used in cases where it is important to detect whether a particular scatterer spacing is present (i.e., discriminate between tissues with regular scatterer spacings in a limited range and tissues with other scattering configurations, such as diffuse and other scatterer spacings).

This paper uses Monte Carlo simulations to quantify the performance relationship between the AR model order and detecting the mean scatterer spacing. Such a relationship provides important information for setting the AR model parameters in a given application and provides a quantitative aspect to the phrase "slightly larger than the scattering spacings" for model order selection. Estimation and detection errors arise primarily from randomness (noise) in the measured signal. The primary noise sources in this application are the variations in scatterer spacings and strengths of the regular tissue, and the backscattered energy from the diffuse scatterers. An increase in each source of randomness degrades the detection performance. The Monte Carlo simulations vary these quantities and estimate the scatterer spacings for each run to observe the range of AR model orders required for reliable detection with the AR cepstral method.

A brief description of the mean scatterer spacing estimator using the AR model is presented in Section II. Section III discusses the simulation and analyzes the merits and limitations of the AR model. Section IV presents an example of applying the AR cepstrum to an actual liver scan to estimate the mean scatterer spacing. Finally, Section V summarizes the criteria for applying the AR model in the detection of mean scatterer spacings.

II. Theory

The tissue structure is modeled as a sparse collection of randomly distributed weak scattering particles, where the effective point scatterers interact only once with the incident pulse as it propagates through the tissue. A scattering function, $x(t)$, models both the regular and diffuse tissue scatterers within the ultrasonic beamfield and is denoted by

$$x(t) = \sum_{n=1}^{N_s} a_n(t = \tau_n) + \sum_{n=1}^{N_D} v_n(t - \theta_n) \tag{1}$$

where t is a time axis (related to the distance by the velocity of the pulse), N_D is the total number of diffuse scatterers, v_n denotes the scattering function for the nth diffuse scatterer, θ_n represents the delay associated with the nth diffuse scattering center, N_S is the total number of regular scatterers, a_n denotes the scattering function for

Manuscript received July 11, 1995; revised March 13, 1996. This paper is based on work supported in part by the National Cancer Institute and the National Institutes of Health Grant PO1-CA52823-05.

T. Varghese is with the Ultrasonics Laboratory, Department of Radiology, University of Texas Medical School at Houston, Houston, TX 77054 USA.

K. D. Donohue is with the Department of Electrical Engineering, University of Kentucky, Lexington, KY 40503 USA (e-mail: donohue@engr.uky.edu).

V. I. Genis is with the Biomedical Engineering and Science Institute, Drexel University, Philadelphia, PA 19104 USA.

E. J. Halpern is with the Division of Ultrasound, Thomas Jefferson University Hospital, Philadelphia, PA 19107 USA.

Publisher Item Identifier S 0885-3010(96)06320-4.

the nth regular scatterer, and τ_n represents the delay associated with the nth regular scattering center.

Attenuation of the propagating ultrasound pulse depends on the scattering and absorption properties of the tissue. A time varying function, $h(t,\tau)$, denotes the illuminating pulse at each scatterer within the beamfield. This function includes the frequency dependent attenuation due to the propagation path to and from the scatterer of interest. The A-scan resulting from the backscattered energy can be written as

$$y(\tau) = \sum_{n=1}^{N_S} \int_{-\infty}^{\infty} h(\tau_n, \tau - \lambda) a_n(\lambda - \tau_n)\, d\lambda + \sum_{n=1}^{N_D} \int_{-\infty}^{\infty} h(\theta_n, \tau - \lambda) v_n(\lambda - \theta_n)\, d\lambda \quad (2)$$

where λ represents the system response axis at a given time τ.

The AR model assumes the observed data result from the output of a linear system excited by a white stationary input sequence [15]. The sampled output sequence $y(n)$ is given by

$$y(n) = -\sum_{k=1}^{p} \alpha_k y(n-k) + w(n) \quad (3)$$

where $w(n)$ is the white noise input sequence to the system, $y(n)$ is the observed data, α_k's are the AR parameters, and p is the order of the model. When the model order is greater than the number of samples between the regular scatterers, the associated power spectrum contains information related to that spacing. In addition, since a white noise input sequence is assumed, the AR parameters also characterize the effects of the frequency dependent (colored) scatterers [$a_n(t)$ and $v_n(t)$] together with the spectrum of the illuminating pulse $h(t,\tau)$. The power spectrum of the output sequence can be written as

$$P_Y(f) = |H_s(f)|^2 P_w(f) \quad (4)$$

where $P_w(f)$ is the power spectrum of the input sequence, and $H_s(f)$ is the frequency response of the model. When $w(n)$ is a zero-mean white noise sequence with variance σ_W^2, the power spectrum of the output sequence has the same form as the system frequency response and is given by

$$P_Y(f) = |H_s(f)|^2 \sigma_w^2 = \frac{|B(f)|^2 \sigma_w^2}{|A(f)|^2} \quad (5)$$

where for the AR model

$$A(f) = 1 + \sum_{k=1}^{p} a_p(k) e^{-j2\pi f k}, \quad B(f) = 1. \quad (6)$$

Since the model order chosen was greater than the scatterer spacing, $H_s(f)$ characterizes the deterministic (or predictable) components of both the regular and diffuse echoes, in addition to the pulse and scatterer characteristics.

Estimation of the power spectrum involves two steps. First, the model parameters (α_k) are estimated from the data sequence $y(n)$ (this paper used Burg's algorithm as in [6] and [11]). Next, the power spectrum is estimated using (5) and (6).

A periodicity in the power spectrum corresponds to a cepstral peak whose location indicates the mean scatterer spacing value. The system response and frequency dependent scattering effects are assumed to be a slowly varying component in the power spectrum, and they primarily contribute to the cepstral regions corresponding to the smaller scatterer spacings (i.e., values within the resolution limit of the system). The effects of the system response are reduced by applying a weighted window along the cepstral axis to suppress these amplitudes. The mean scatterer spacing is computed from the location (Δt) of the dominant peak in the cepstrum using

$$d = \frac{V \Delta t}{2} \quad (7)$$

where V denotes the velocity of the propagating ultrasound pulse.

TABLE I
SIMULATOR SPECIFICATION

Simulation Specifications	Value
Absorption Coefficient	0.94 dB cm^{-1}
Scattering Coefficient at 180^0, measured at 3 MHz	9 x 10^{-4} Sr^{-1} cm^{-1}
Diffuse Scatterer size	10 μm
Regular Scatterer size	80 μm
Pulse Center Frequency	3.5 MHz
Pulse 3 dB Bandwidth	1.9 MHz
Sampling rate	24 MHz
Propagation velocity	1540 m/s

A mean scatterer spacing can be resolved when the correlation length of the propagating ultrasonic pulse is shorter than the spacing between individual scatterers. The effective resolution of the received echo imposes a limitation on the smallest resolvable scatterer spacing [10], while the model order limits the largest detectable scatterer spacing. In addition to these limitations on the measurement system, the error associated with the algorithm further limits the range of detectable scatterer spacings. Monte Carlo simulations presented in the next section reveal the additional limitations due to the AR model.

III. SIMULATION

A-scans for the simulation experiment are obtained from (2) using known tissue and signal parameters. Tissue parameters for the simulation were chosen from experimental research with human liver tissue *in vitro* [12]–[14]. Scatterer spacings were simulated using a Gamma distribution for cases with very irregular spacings and cases with almost deterministic spacings (scatterer spacing standard deviations ranged from 3.14 to 9.99% of the mean scatterer spacing). The radial positions of the diffuse scatterers were uniformly distributed throughout the beamfield of the ultrasound pulse. The scatterer number was determined using a Poisson deviate and chosen to simulate Gaussian statistics for the scatterer number (about 15–20 scatterers per resolution cell). The scatterer strengths for both the regular and diffuse scatterers follow a uniform distribution. The fluctuations in the scatterer strength are intended to model changes in the orientation and strength of the scatterers within the beamfield. The uniform distribution for the scatterer strength is somewhat extreme, as a collection of regular scatterers would tend to have a central tendency in echo strength (although a very large variance is possible). The uniform model, however, represents a worse case for the amplitude modulation of the regular scatterers in the real tissue. The initial system response, $h(t)$, is attenuated as the pulse propagates through the tissue and is initially modeled with a Gaussian-shaped envelope. Table I presents the parameters used in the simulation experiment.

The signal-to-noise ratio (SNR) used in this paper represents the power ratio between the regular and diffuse components and is computed as follows:

$$\text{SNR} = 10 \log \left[\frac{\int_0^{\Delta t} \left(\sum_{n=1}^{N_S} \int_{-\infty}^{+\infty} h(\tau_n, \tau = \lambda) a_n(\lambda - \tau_n)\, d\lambda \right)^2 d\tau}{N_S \int_0^{\Delta t} \left(\sum_{n=1}^{N_D} \int_{-\infty}^{+\infty} h(\theta_n, \tau - \lambda') v_n(\lambda - \theta_n)\, d\lambda \right)^2 d\tau} \right] \quad (8)$$

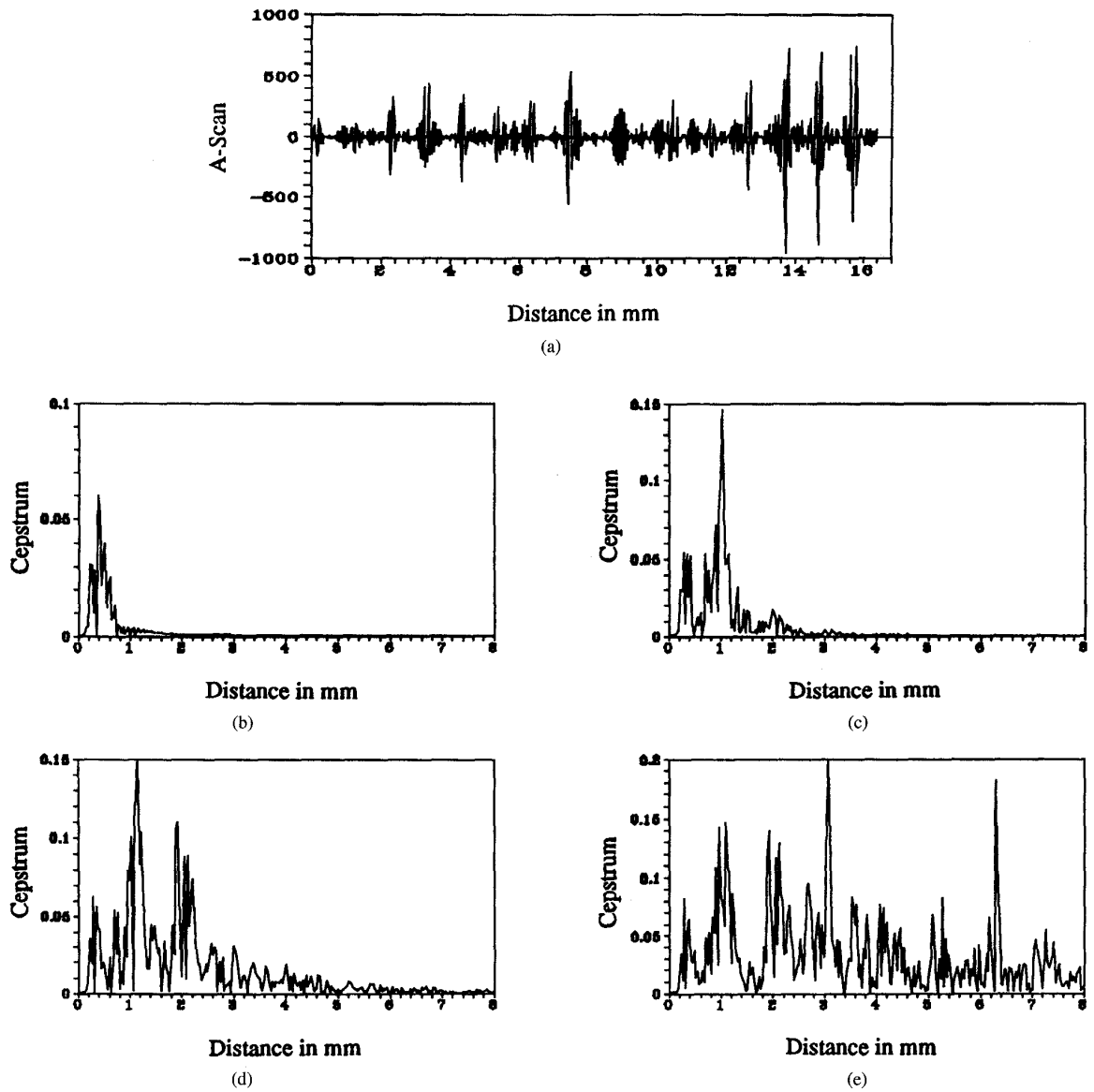

Fig. 1. A-scan and the AR-cepstra for different orders of the AR model. (a) A-scan segment. (b) AR-cepstrum with $p = 10$. (c) AR-cepstrum with $p = 40$. (d) AR-cepstrum with $p = 80$. (e) AR-cepstrum with $p = 200$.

where Δt is the length of the data segment. The factor N_S is included in the denominator to account for the number of regular scatterers over the Δt interval. Without this factor, the SNR would increase with the number of scatterers (N_S), rather than directly relate to the strength of the scattering functions. In this manner the SNR represents a per-regular-scatterer value, independent of the spacing. This paper presents results for only one SNR value. An SNR of 4 dB was determined to be close to the limit for reliable output for the AR method as applied here [11]. Thus, better results can be expected for signals with higher SNR and/or more consistency in the amplitudes of the regular scatterer spacings. As the SNR degrades, the detection becomes unreliable. In actual tissues, a wide range of SNR values exists due to variability in the strengths and orientations of the regular scatterers. For a general application to real tissue, if the quasi-periodic scatterers are visibly observable, then the AR method should provide reliable detection. In cases where these scatterers are difficult to observe, the AR method will generate excessive spurious peaks. In these cases spectral correlation methods should be used [10], [11]; however, the resolution with this approach is limited.

Fig. 1 presents a simulated A-scan segment with an SNR of approximately 4 dB and its corresponding AR-cepstra for different AR model orders. The A-scan was simulated using an average scatterer spacing of 1.02 mm and standard deviation (σ) equal to 3.14% of the mean scatterer spacing. A mean spacing of 1.02 mm corresponds to 32 samples in this case, and for all cases the AR coefficients were computed from a data segment of 512 samples. Note that the true value of the spacing is properly indicated as shown in Fig. 1(c) and (d) corresponding to model orders 40 and 80, respectively. The AR model order of 10, shown in Fig. 1(b), does not span the distance of the mean scatterer spacings; hence, it is unable to detect the quasi-periodic scatterer spacing. The model order $p = 40$ provides the strongest cepstral peak at 1 mm. Notice in Fig. 1(d) that

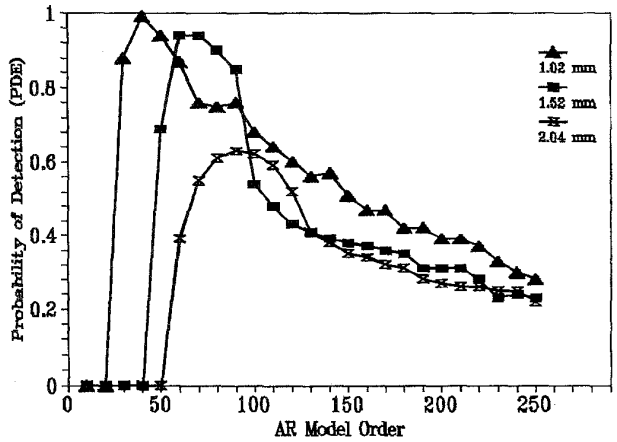

Fig. 2. Probability of detection with a probability of false alarm of 0.001, for regular scatterers with σ of 3.14%.

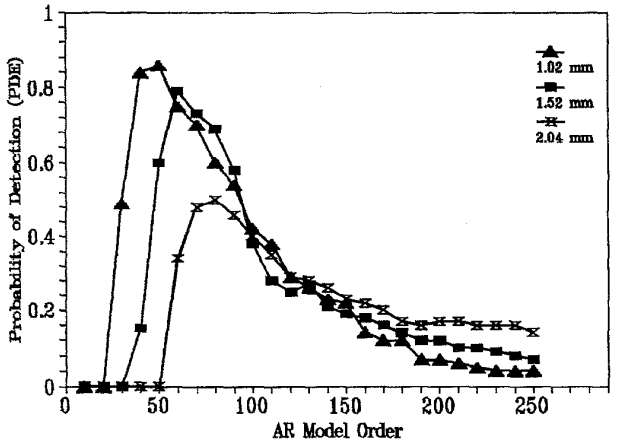

Fig. 3. Probability of detection with a probability of false alarm of 0.001, for regular scatterers with σ of 9.99%.

as the order is increased to 80, the number of spurious peaks increases. While the true value of the spacing is still the dominant peak in this case, for other A-scans simulated with these same parameters, the peak at 2 mm dominates the cepstrum. This demonstrates the tendency of the AR cepstrum to generate spurious peaks driven by either noise or harmonics of the underlying spacing. As the order is increased to 200, shown in Fig. 1(e), the cepstral peak corresponding to the true value of the scatterer spacing is masked by the occurrence of the spurious peaks due to increased estimation errors of the AR coefficients associated with larger model orders (over a fixed data segment).

The previous example illustrated the need to set the proper model order and to limit spurious peaks, which can lead to incorrect conclusions concerning the data. The following performance analysis examines the ability of the AR method to generate a dominant peak in the correct location when regular spacings exist, while limiting spurious peaks when diffuse-only data are present (or when a regular scatterer spacing does exist, limiting the spurious peaks at other locations). The probability of detection (PDE), therefore, is used to compare relative performances as a function of model order, under the constraint of a constant probability of false alarm (PFA). A threshold corresponding to a constant PFA is determined, and the detection probability is computed from the simulation. This approach simplifies the threshold design problem since it requires only the statistics on the cepstral peaks corresponding to noise. In this paper an exponential cumulative distribution function (cdf) is used to describe the cepstral amplitude variations, and is given by

$$P(x) = 1 - \exp(x/C_{\text{avg}}) \qquad 0 \le x \le \infty \tag{9}$$

where C_{avg} is the mean of the cepstral values resulting from the diffuse scatterers. While the spectral magnitude for diffuse scattering can be considered exponential [7], the logarithm is not. The DFT operation, however, used to obtain the final cepstrum, performs a summing operation that (due to the central limit theorem) transforms the distribution toward an exponential. This was observed through comparing histograms for many of the diffuse-only cepstra. In the simulation, C_{avg} was estimated from the data and substituted into (9). The PFA threshold for the exponential distribution is determined by setting $P(x)$ from (9) equal to 1-PFA and solving for the variable x. This value of x is the threshold denoted by t_{FA}, which reduces to

$$t_{\text{FA}} = C_{\text{avg}}\left(\ln \frac{1}{\text{PFA}}\right) \qquad 0 < \text{PFA} \le 1 \tag{10}$$

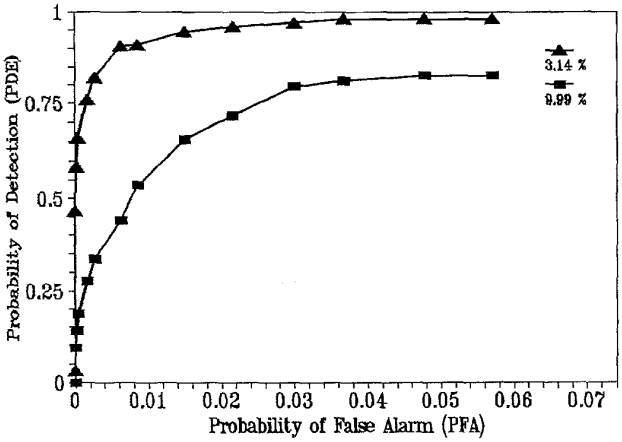

Fig. 4. Receiver operator characteristic curves for regular scatterers with an SNR of 4 dB and σ = 3.14 and 9.99%.

where C_{avg} is the average computed from regions not associated with the scatterer spacings.

For all the constant PFA plots presented in this paper, the PFA was also computed to confirm that the resulting PFA was well within an order of magnitude of the designed threshold's false alarm probability. Such accuracy is sufficient for the relative comparisons of optimal AR model orders presented in Figs. 2 and 3. The relation between the computed PDE and PFA for a series of thresholds is presented later as receiver operator characteristics (ROC) (see Fig. 4).

A cepstral peak exceeding the threshold is considered a detection if it lies within a region corresponding to three standard deviations of the underlying scatterer spacings extending from either side of the actual mean square spacing. Cepstral peaks outside this window are considered spurious or noise peaks, and when they cross the threshold, they become false alarms. Note that a detection does not imply much about the quality of the estimate, since the window for the location is relatively large. Before dealing with issues related to estimation quality, however, it is important to establish that the peak from which the estimate is derived results from the phenomenon of interest rather than a spurious peak driven by noise.

The AR method is used to compute the mean scattering spacing for simulated A-scans with scatterer spacings of 1.02, 1.52, and 2.04 mm, respectively. The Monte Carlo simulation generated over 100

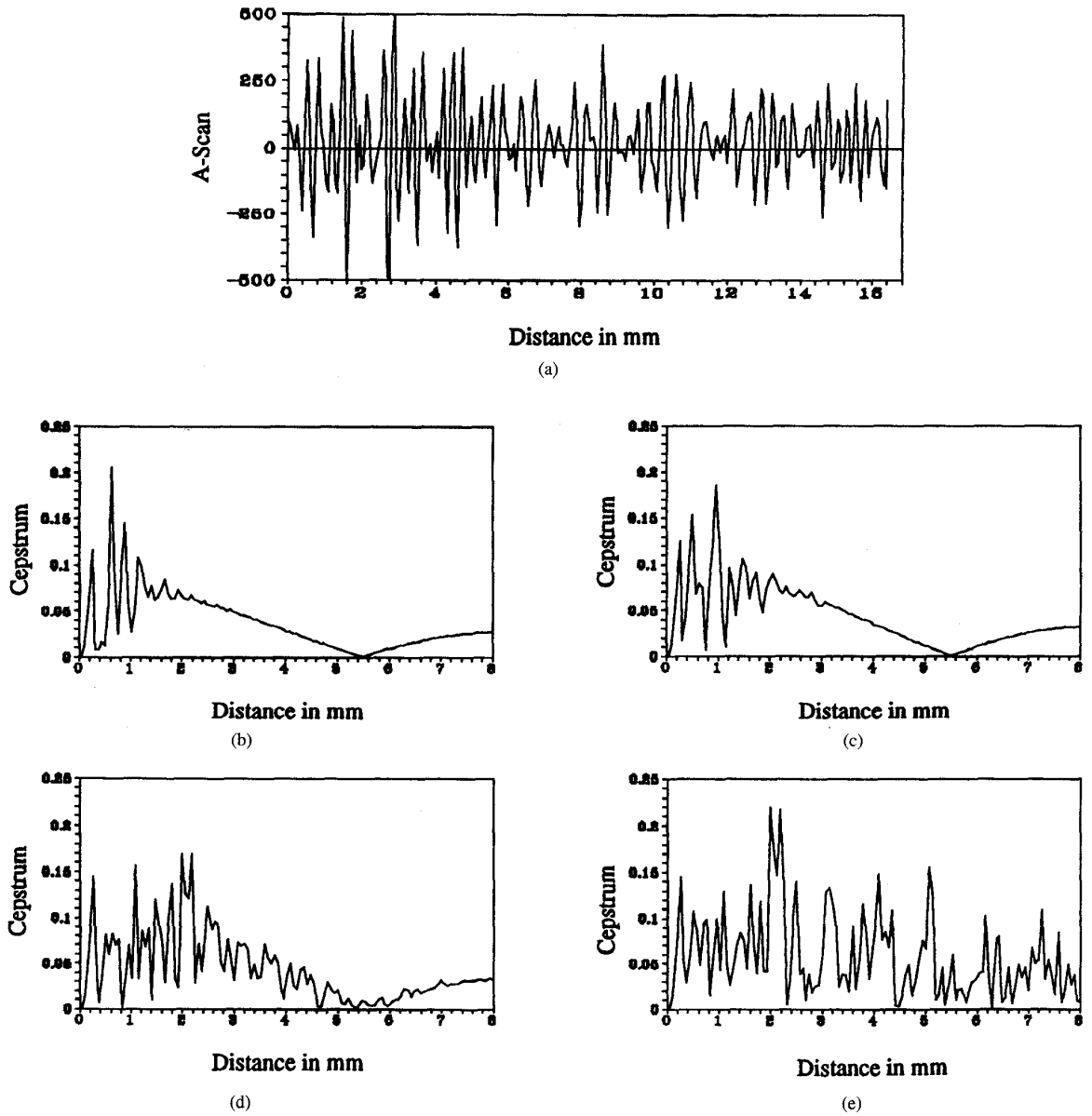

Fig. 5. A-scan and the AR-cepstra for liver tissue for different orders of the AR model. (a) A-scan segment. (b) AR-cepstrum with $p = 10$. (c) AR-cepstrum with $p = 20$. (d) AR-cepstrum with $p = 40$. (e) AR-cepstrum with $p = 100$.

simulated A-scans with an SNR of 4 dB for each plotted point. Each data segment was of length 16 mm (512 sample points). The order of the AR model was varied from 10 to 250 in increments of 10. Simulation results presented in Figs. 2 and 3 show the PDE as a function of model order.

The PDE plots in Figs. 2 and 3 indicate that the best performance occurs when the AR model order is about 25% greater than the true scatterer spacing. For consistent detection performance over a range of spacings, the underlying mean scatterer spacings variations should be limited to $\pm 5\%$ of the scatterer spacing with which the model order was determined. Performance quickly degrades for scatterer spacings outside this range. Also note from Figs. 2 and 3 that the PDE further reduces when the model order is greater than 100 $(N/5)$ for all cases. This is observed by the decrease in the PDE at the optimal point for increased scatterer spacings (requiring higher orders). An increase in the order of the AR model, for a fixed set of data points, results in less statistical averaging for the AR coefficient estimation. These errors cause the formation of more spurious peaks in the AR cepstrum, thereby increasing the level of the constant PFA threshold and reducing the PDE. This is evident even for AR model orders larger than 70. The PDE reduces from 0.99 for the 1.02 mm spacing to 0.63 for the 2.04 mm spacing with $\sigma = 3.14\%$. A comparison between the PDE in Figs. 2 and 3 also shows a performance reduction with an increase in standard deviation of the regular scatterer spacings (from 0.99 with $\sigma = 3.14\%$ to 0.86 with $\sigma = 9.99\%$ for a scatterer spacing of 1.02 mm).

The ROC curves for scatterers with a spacing of 1.02 mm for two different σ values are presented in Fig. 4 for the optimum AR model order of 40 over 200 simulated A-scans. These plots indicate that the PDE increases slowly (plateaus off) for thresholds corresponding to

PFA equal to 0.03 and above. Therefore, if a false alarm rate of 3 out of 100 or greater can be tolerated, a close-to-maximum PDE can be obtained. Note the overall reduction in the PDE with an increase in the standard deviation (σ) of the regular scatterers, from 0.98 for $\sigma = 3.14\%$ to 0.82 for $\sigma = 9.99\%$.

IV. Clinical Results

In this section data from *in vivo* scans of liver tissue are used to illustrate the estimation of the mean scatterer spacing using AR cepstral analysis. B-scan images of the liver were obtained using the Ultramark 9 ultrasound system (ATL, Bothell, WA). The individual RF A-scans were directly obtained from this system using a transducer with a center frequency $f_c = 3.5$ MHz, 3 dB bandwidth $f_{3\text{dB}} = 2.0$ MHz and a sampling frequency $f_s = 12$ MHz. An antialiasing filter with a cutoff frequency of 6 MHz was applied to each A-scan before sampling.

Fig. 5 presents an A-scan segment from the liver tissue, along with the AR cepstrum for different model orders. Relative to the simulated A-scan, the scan from the liver tissue appears to have a lower SNR. In both scans, however, a quasi-periodic series of echoes is observed (note that the simulated data were sampled at twice the rate of the real data; this accounts for the more dense appearance). Observe that the dynamic range for the scatterer amplitudes in the simulation is greater than the series of scatterers from the particular liver tissue segment. A high-variance random modulation of the regular scatterer amplitudes makes the detection problem more difficult since the periodic frequency components in the frequency domain are smeared out by a convolution with a relatively broad spectrum. When the regular scatterer amplitudes are more consistent, as in the liver segment shown, the detection becomes easier and a better detection performance can be expected. Overall, there are some segments in the liver where a large dynamic range of echoes is found and other regions where no regular scatterer spacing is observed. This example was picked for demonstration because it fit the rule stated earlier, that the quasi-periodic scatterers should be observed visually for the AR method to generate reasonable results. Therefore the effect of order selection on a detectable data segment is observed.

A data segment of length 16 mm (256 data points) was extracted, and the AR method with model orders of 10, 20, 40, and 100 was applied. The characteristic 1 mm spacing can be observed in the AR cepstrum for $p = 20$, as shown in Fig. 5(c). For a periodic spacing of 1 mm, the true scatterer locations are separated by an average of 16 sampled data points for a sampling frequency of 12 MHz. Fig. 5(b) indicates that the AR model order of 10 is unable to detect clearly the correct value of the scatterer spacing (it detects a spacing near 0.7 mm, which is close to the resolution limit of the system). The cepstral peak due to the 1 mm spacing can be observed for $p = 40$, as shown in Fig. 5(d). The dominant cepstral peak, however, occurs at a spacing near 2 mm. The 2 mm spacing can also be observed for a model order $p = 100$ in Fig. 5(e). Note also the increase in the number of spurious peaks as the orders increase from 10 to 100 in Fig. 5 (see Fig. 1 to observe similar patterns in the simulation). This is consistent with the relation observed in the simulation that the PDE significantly decreases due to spurious peaks as the order increases beyond $N/5$, where N is the length of the data segment.

V. Conclusion

This paper presented a PDE analysis on AR model order for detecting the mean scatterer spacing. For optimal detection of the scatterer spacing, the order of the AR model should span a length approximately 25% larger than the expected scatterer spacing. In addition, the detection range of scatterer spacings is limited to $\pm 5\%$ of the expected scatterer spacings. The PDE reduces significantly (by about 25%) with an increase in the variance of the underlying regular scatterers (from 3.14 to 9.99%) as indicated by the ROC results. In addition, for the SNR values used in this paper, the data segment length should be at least five times the model order to limit the spurious peaks.

The AR model can provide good reliability in detecting scatterer spacings when the expected spacing range is known. Better results can be expected for signals with SNR values higher than 4 dB and/or more consistent scatterer strengths for the regular scatterers. This paper considered detection error only in determining the range of models orders for consistent performance. This work did not, however, examine the accuracy of estimation within the reliable detection performance range. The estimation accuracy must also be examined with appropriate noise models to determine the degree to which the high-resolution properties of the AR model can be exploited in estimating the scatterer spacings.

References

[1] M. F. Insana, R. F. Wagner, D. G. Brown, and T. J. Hall, "Describing small-scale structure in random media using pulse-echo ultrasound," *J. Acoust. Soc. Amer.*, vol. 87, pp. 179–192, 1990.

[2] L. L. Fellingham and P. G. Sommer, "Ultrasonic characterization of tissue structure in the *in vivo* human liver and spleen," *IEEE Trans. Sonics Ultrason.*, vol. SU-31, pp. 418–428, 1984.

[3] B. S. Garra, K. A. Wear, R. F. Wagner, M. F. Insana, and T. J. Hall, "Quantitative ultrasonic detection and classification of diffuse liver diseases," *Invest. Radiol.*, vol. 24, no. 3, pp. 196–203, 1989.

[4] L. Landini and L. Verrazzani, "Spectral characterization of tissue microstructure by ultrasound: A stochastic approach," *IEEE Trans. Ultrason., Ferroelect., Freq. Contr.*, vol. 37, pp. 448–456, 1990.

[5] R. Kuc, K. Haghkerder, and M. O'Donnell, "Presence of cepstral peaks in random reflected ultrasound signal," *Ultrason. Imag.*, vol. 8, pp. 196–212, 1986.

[6] K. A. Wear, R. F. Wagner, M. F. Insana, and T. J. Hall, "Application of auto-regressive spectral analysis to cepstral estimation of mean scatterer spacing," *IEEE Trans. Ultrason., Ferroelect., Freq. Contr.*, vol. 40, pp. 50–59, Jan. 1993.

[7] R. F. Wagner, M. F. Insana, and D. G. Brown, "Unified approach to the detection and classification of speckle texture in diagnostic ultrasound," *Opt. Eng.*, vol. 25(6), pp. 738–742, 1986.

[8] M. F. Insana, R. F. Wagner, B. S. Garra, D. G. Brown, and T. H. Shawker, "Analysis of ultrasound image texture via generalized Rician statistics," *Opt. Eng.*, vol. 25(6), pp. 743–748, 1986.

[9] T. Varghese and K. D. Donohue, "Characterization of tissue microstructure scatterer distribution with spectral correlation," *Ultrason. Imag.*, vol. 15, pp. 238–254, 1993.

[10] ——, "Mean scatterer spacing estimates with spectral correlation," *J. Acoust. Soc. Amer.*, vol. 96, no. 6, pp. 3504–3515, Dec. 1994.

[11] ——, "Estimation of the mean scatterer spacing estimatesusing the frequency-smoothed spectral autocorrelation function," *IEEE Trans. Ultrason., Ferroelect., Freq. Contr.*, vol. 42, pp. 451–463, May 1995.

[12] L. R. Romijn, J. M. Thijssen, and G. W. J. Van Beuningen, "Estimation of scatterer size from backscattered ultrasound: A simulation study," *IEEE Trans. Ultrason., Ferroelect., Freq. Contr.*, vol. 36, pp. 593–605, Nov. 1989.

[13] J. C. Bamber, C. R. Hill, and J. A. King, "Acoustic properties of normal and cancerous human liver—II, Dependence on tissue structure," *Ultrasound Med. Biol.*, vol. 7, pp. 135–144, 1981.

[14] D. Nicholas, "Evaluation of backscattering coefficients for excised human tissue: Results, interpretation and associated measurements," *Ultrasound Med. Biol.*, vol. 8, pp. 17–28, Aug. 1982.

[15] J. G. Proakis and D. G. Manolakis, *Digital Signal Processing, Principles, Algorithms and Applications*, 2nd ed. New York: Macmillan, 1992.